Biochimica et Biophysica Acta 1794 (2009) 1218–1223

Contents lists available at ScienceDirect

Biochimica et Biophysica Acta

journal homepage: www.elsevier.com/locate/bbapap

Structural and kinetic analysis of *Saccharomyces cerevisiae* thioredoxin Trx1: Implications for the catalytic mechanism of GSSG reduced by the thioredoxin system

Rui Bao [b,1], Yaru Zhang [b,1], Xiaochu Lou [b], Cong-Zhao Zhou [a], Yuxing Chen [a,b,*]

[a] Hefei National Laboratory for Physical Sciences at Microscale and School of Life Sciences, University of Science and Technology of China, Hefei, Anhui 230026, People's Republic of China
[b] Institute of Protein Research, Tongji University, Shanghai 200092, People's Republic of China

ARTICLE INFO

Article history:
Received 24 January 2009
Received in revised form 28 March 2009
Accepted 1 April 2009
Available online 9 April 2009

Keywords:
Thioredoxin system
Yeast
Glutathione
Kinetic parameters
Reduction efficiency

ABSTRACT

Thioredoxin (Trx) and glutathione/glutaredoxin (GSH/Grx) systems play the dominant role in cellular redox homeostasis. Recently the Trx system has been shown to be responsible to control the balance of GSH/GSSG once the glutathione reductase system is not available. To decipher the structural basis of electron transfer from the Trx system to GSSG, we solved the crystal structures of oxidized Trx1 and glutathionylated Trx1Cys33Ser mutant at 1.76 and 1.80 Å, respectively. Comparative structural analysis revealed a key residue Met35 involved in the Trx-GSSG recognition. Subsequent mutagenesis and kinetic studies proved that Met35Arg mutation could alter the apparent K_m and V_{max} values of the reaction. These findings gave us the structural insights into GSSG reduction catalyzed by the Trx system.

1. Introduction

Thioredoxin (Trx) is a small redox active protein with a conserved catalytic active motif (-Trp-Cys-Gly-Pro-Cys-) that undergoes reversible oxidation–reduction of two thiol groups. Trx functions as the electron donor for ribonuleotide reductase [1], 3′-phosphoadenosine-5′-phosphosulfate reductase [2], protein methionine sulfoxide reductase [3] and Trx-dependent peroxidases [4] etc. Trx is also a potent universal reductant against disulfides in low-molecular-weight compounds [5].

The Trx system, together with the glutathione/glutaredoxin (GSH/Grx) system, plays an important role in maintaining the cellular redox homeostasis [6]. GSH is the most abundant low-molecular-weight thiol [7], and its ratio to the oxidized form GSSG is mainly maintained by glutathione reductase (GR) [8]. However, absence of GR in some species such as fruit fly has been reported, indicating the important role of Trx system in the homeostasis of GSH/GSSG [9]. Recent studies mainly focused on the *in vitro* activity of the Trx system towards GSSG [9,10], leaving the information concerning the reaction intermediate largely unknown.

The yeast *Saccharomyces cerevisiae* contains a cytoplasmic (Trx1/2 and Trr1) [11,12] as well as an intact mitochondrial Trx system (Trx3 and Trr2) [13]. In *S. cerevisiae*, a lethal genetic screen for the null mutant of GR showed an overlapping role between Trx and Grx systems [14]. Further reports revealed that GSSG would be accumulated in cells deficient of both *TRX1* and *TRX2* [15]. In fact, the regulation of the two systems is not reciprocal that independent redox regulation of Trxs could enable cells to survive in conditions under which the GSH/Grx system is over-oxidized [16]. It seems that the GSH/GSSG ratio is modulated by the yeast Trx system, but the GSSG-reducing rate is unclear.

Thus, we tested the apparent second-order rate constant k_2 of reduced Trx1 towards GSSG, which characterizes the chemical reaction between the Trx system and GSSG by the following reaction sequence:

$$\mathrm{NADPH} + \mathrm{TrxS_2} + \mathrm{H^+} \xrightarrow{k_1} \mathrm{NADP^+} + \mathrm{Trx(SH)_2} \qquad \text{(Reaction 1)}$$

$$\mathrm{Trx(SH)_2} + \mathrm{GSSG} \xrightarrow{k_2} \mathrm{TrxS_2} + 2\ \mathrm{GSH}. \qquad \text{(Reaction 2)}$$

The measured k_2 value in Reaction 2 (6 mM^{-1} min^{-1}) is similar to the previous data from *Escherichia coli* (6 mM^{-1} min^{-1}) [17] and *Drosophila melanogaster* (10 mM^{-1} min^{-1}) [9], but these values are much lower than that from *Plasmodium falciparum* (39 mM^{-1} min^{-1}) [10]. Considering the high level of sequence identity among thioredoxins from these species (40% to 48%), and the absolute conservation of the active site, the discrepancy should be resulted from some subtle structural variations. In an attempt to clarify this puzzle, we solved the crystal structures of oxidized Trx1 and glutathionylated Trx1C33S mutant (Cys33 is the C-terminal cysteine residue of the active site).

Comparisons of primary and tertiary structures of thioredoxins from several species revealed the essential residues which may

* Corresponding author. Hefei National Laboratory for Physical Sciences at Microscale and School of Life Sciences, University of Science and Technology of China, Hefei, Anhui 230026, People's Republic of China.
E-mail address: cyxing@ustc.edu.cn (Y. Chen).
[1] Both authors contributed equally to this work.

1570-9639/$ – see front matter © 2009 Elsevier B.V. All rights reserved.
doi:10.1016/j.bbapap.2009.04.001

account for their divergent reaction rate constants towards GSSG. Of these residues, Met35 (number according to yeast Trx1) is the most important. Thus the mutant of Met35Arg was constructed, and the subsequent activity assays provided us more insights into the mechanism of Trx-GSSG reduction.

2. Materials and methods

2.1. Cloning, expression and purification

The coding sequences of yeast Trx1/YLR043C and Trr1/YDR353W were constructed in pET28-derived vector as described elsewhere [18,19] and the Trx1C33S (Cys33/Ser33 mutation) and Trx1M35R (Met35/Arg35 mutation) mutants were obtained by site-directed mutagenesis. All recombinant proteins with 6× His-tag at the N-terminus were overexpressed in *E. coli* BL21 (DE3) strain, and subjected to Ni-NTA affinity column followed by gel filtration with Superdex-75 or Superdex-200 (GE healthcare) for further purification. The glutathionylated Trx1C33S (gsTrx1C33S) was prepared as described [20]. All proteins used for the activity assay were purified with the buffer containing 100 mM sodium chloride, 20 mM Tris–HCl, pH 8.0.

2.2. Crystallization, data collection, structure solution and refinement

The initial crystal screening trial was made with Hampton Research Kit 1&2. The ultimate conditions for the growth of crystals suitable for X-ray diffraction were 4% PEG 400, 12% PEG 8000, 0.1 M sodium acetate pH 4.6 and 0.2 M zinc acetate for Trx1 [18] and 2.2 M ammonium sulfate, 0.1 M sodium acetate pH 4.4 for gsTrx1C33S [20] by hanging-drop vapor-diffusion method at 289 K. Diffraction data were collected at 100 K on an in-house Rigaku MM007 X-ray generator ($\lambda = 1.54180$ Å) with a MarResearch 345 detector at School of Life Sciences, University of Science and Technology of China (USTC, Hefei, PR China).

The data were indexed and integrated with MOSFLM [21] and scaled by SCALA [22] of CCP4 suite 6.0.2 [23]. The homology model was generated from Trx2 (PDB code: 2FA4) [24]. The structures were solved by molecular replacement with the program MOLREP [23,25] followed by rigid body refinement and restrained refinement in REFMAC5 [23,26]. Alternatively, manual rebuilding and water relocation were performed with COOT [27]. The stereochemistry of the models was calculated with PROCHECK and MolProbity [23,28]. Final coordinates and structure factors have been deposited in Protein Data Bank (www.rcsb.org) under the accession code of 3F3Q and 3F3R. The data collection and refinement statistics were summarized in Table 1.

2.3. Activity assay

The activity of *S. cerevisiae* Trr1 towards Trx1 or Trx1M35R was determined by the DTNB (5,5′-dithiobis(2-nitrobenzoic acid)) assay, which was performed as described previously [29]. Briefly, the reaction mix of 200 μl containing 100 mM phosphate buffer, pH 7.5, 4 mM EDTA, 1 mM DTNB, 0.5 mM NADPH and various concentrations of Trx from 0.2 to 14 μM were triggered by adding 10 nM Trr1. The absorbance at 412 nm was monitored for 5 min at 25 °C (Beckman-Coulter DU800).

The reducing activity of Trx1 or Trx1M35R towards GSSG was detected by monitoring the decrease of absorbance at 340 nm due to the oxidation of NADPH. The 200 μl reaction mix containing 100 mM phosphate buffer (pH 7.5), 4 mM EDTA, 250 μM NADPH, 200 nM Trr1, 5 μM Trx1 or Trx1M35R was started by the addition of GSSG, ranging from 0.05 to 5 mM. An alternative method was also employed to get the k_2 value of the reaction, as described previously [10]. Briefly, the reaction mix contains 100 mM phosphate buffer, pH 7.5, 4 mM EDTA, 250 μM NADPH, 10 nM Trr1, 5–20 μM Trx1 or Trx1M35R and 20 μM GSSG. The absorbance at 340 nm was recorded for 5 min at 25 °C.

Table 1
Data collection and crystallographic statistics.

	Oxidized Trx1 (Trx1-ox)	Glutathionylated Trx1 (gsTrx1C33S)
Data processing		
Space group	$P2_12_12_1$	$P1$
Unit cell parameters		
a, b, c (Å)	32.29, 46.59, 64.20	38.53, 38.81, 41.70
α, β, γ(°)	90, 90, 90	72.91, 87.51, 60.58
Resolution (Å)	28.85–1.76 (1.83–1.76)[a]	33.32–1.80 (1.90–1.80)
Unique reflections	10,873 (1058)	17,174 (2416)
Completeness (%)	99.0 (96.4)	93.5 (89.28)
$I/\sigma(I)$	23.6 (4.0)	31.89 (11.95)
R_{merge}[b] (%)	4.0 (22.9)	4.0 (7.0)
Refinement statistics		
Resolution (Å)	28.85–1.76 (1.81–1.76)	33.32–1.80 (1.85–1.80)
R_{work}[c]	0.20 (0.30)	0.19 (0.19)
R_{free}[d]	0.25 (0.36)	0.22 (0.26)
Contents of asymmetric unit		
Protein atoms	848	1621
Water atoms	77	132
RMSD[e] geometry		
Bond lengths (Å)	0.016	0.009
Bond angles (°)	1.551	1.195
Average of B-factors (Å^2)	26.25	10.89
Wilson B-factors	23.07	13.7
Protein	25.46	9.64
Water	34.85	18.76
Glutathionyl moiety		29.89
Ramachandran plot[f]		
Most favored (%)	97.20	98.54
Additional allowed (%)	2.80	1.46
Outliers (%)	0	0
PDB entry	3F3Q	3F3R

[a] The values in parentheses refer to statistics in the highest bin.
[b] $R_{merge} = \sum hkl \sum i |Ii(hkl) - \langle I(hkl)\rangle| / \sum hkl \sum i Ii(hkl)$, where Ii(hkl) is the intensity of an observation and $\langle I(hkl)\rangle$ is the mean value for its unique reflection; Summations are over all reflections.
[c] R-factor $= \sum h |Fo(h) - Fc(h)| / \sum h Fo(h)$, where Fo and Fc are the observed and calculated structure–factor amplitudes, respectively.
[d] R-free was calculated with 5% of the data excluded from the refinement.
[e] Root mean square deviation from ideal values.
[f] Categories were defined by Molprobity.

The kinetic constants of the two activity assay systems were determined with OriginPro 7.5 by fitting to the Hill equation with a Hill coefficient of 1. For the alternative method, considering Trx as an electron shuttle, the rate constant between Trx and GSSG can be determined as below [10]:

$$k_2 = \frac{v^*(V_{max} - v)}{[GSSG]^*[Trx_{total}]^*(V_{max} - v) - K_m{}^*v}. \quad (1)$$

V_{max} represents the maximum reaction rate of Trr1 towards Trx1, as determined by the DTNB method, while K_m is the Michaelis–Menten constant of Trr1 towards Trx1, and v stands for the measured reaction rate of Trx1 towards GSSG at the corresponding concentration.

Although the above mentioned kinetic analysis system can help to determine the reaction rate constant k_2, little concerning the reaction process is revealed. Thus a different activity assay system was employed to determine the K_m' and k_{cat}' (the kinetic parameters for Trx-GSSG reaction were indicated with a prime) values of Trx towards GSSG.

All proteins used for activity assay were quantified according to the molar extinction coefficient, ε280 nm of 24,600 and 10,220 $M^{-1}cm^{-1}$ for Trr1 and Trx1, respectively.

3. Results and discussion

3.1. Overall structure and comparison between Trx1 and gsTrx1C33S

The crystal structures of Trx1 in the oxidized form (Trx1-ox) and Cys33/Ser33 mutant covalently linked to a GSH (gsTrx1C33S) were

refined to 1.76 Å and 1.80 Å, respectively. The crystal of Trx1-ox belongs to the space group of $P2_12_12_1$ with one molecule in an asymmetric unit, while gsTrx1C33S to the space group *P1* with two molecules (Table 1). The GSH molecule forms a disulfide bond with Cys30 as clearly presented in the gsTrx1C33S structure (Fig. 1A). The high quality of electron density map even allowed the precise assignment of the N-terminal hexahistidine tag in the Trx1-ox structure.

The overall fold of Trx1 resembles the previously reported NMR structure of yeast Trx1[30], and crystal structures of yeast Trx2 [24] and Trxs from other sources [31–33], consisting of five mixed β-strands flanked by four α-helices (Fig. 2A). The active site is located at the second α-helix and the loop that precedes it. The distance between Sγ atoms of Cys30 and GSH cysteinyl in gsTrx1C33S is 2.30 Å. Different from GSH-bound glutaredoxins in Protein Data Bank (www.rcsb.org), such as the glutathionylated yeast glutaredoxin 1 (gsGrx1, PDB code: 3C1S) [34], this is the first structure of the GSH-bound thioredoxin without the previously defined GSH binding groove. Moreover, Trx1C33S and GSH have much less interactions compared with the structure of gsGrx1 [34]. Only two main chain hydrogen bonds were found between the amino and oxygen atoms of cysteinyl moiety of GSH and Met72-O and -N, respectively (Fig. 2B). The GSH-like Trx recognizing motif (Glu-Cys-Gly) has also been reported in the C-terminal catalytic domain of PAPS reductase [2], which has specific interaction with Trx. Although the interactions are weaker than those in GSH-bound glutaredoxins, GSSG could be transiently recognized by Trx. This rather dynamic interaction between Trx and GSSG results in a much higher B-factor of the GSH molecule compared to the average B-factor of Trx1C33S, whereas the GSH and Grx1 in the gsGrx1 structure have a similar B-factor. Thus the structure depicts an intermediate complex with the product GSH ready to be released. Despite sharing a great structural similarity, especially at active site, with Grx1, Trx1 serves as a less active deglutathionylation agent, but a much better reducing agent towards GSSG.

Structural superposition of Trx1-ox against gsTrx1C33S gives an overall Cα RMSD (root mean square deviation) of 0.75 Å. The B-factors of the region Lys34-Pro38 in Trx1-ox are higher than that of the active site, whereas the corresponding region in gsTrx1C33S and the active site have similar B-factors. There are conformational differences between the glutathionylated Trx1Cys33Ser mutant and the oxidized Trx1 at the second active site cysteine and succeeding segment (Cys33/Ser33-Pro38) (Fig. 2B). The side chains of Lys34 and Met35 shift to the opposite direction of GSH in gsTrx1C33S structure,

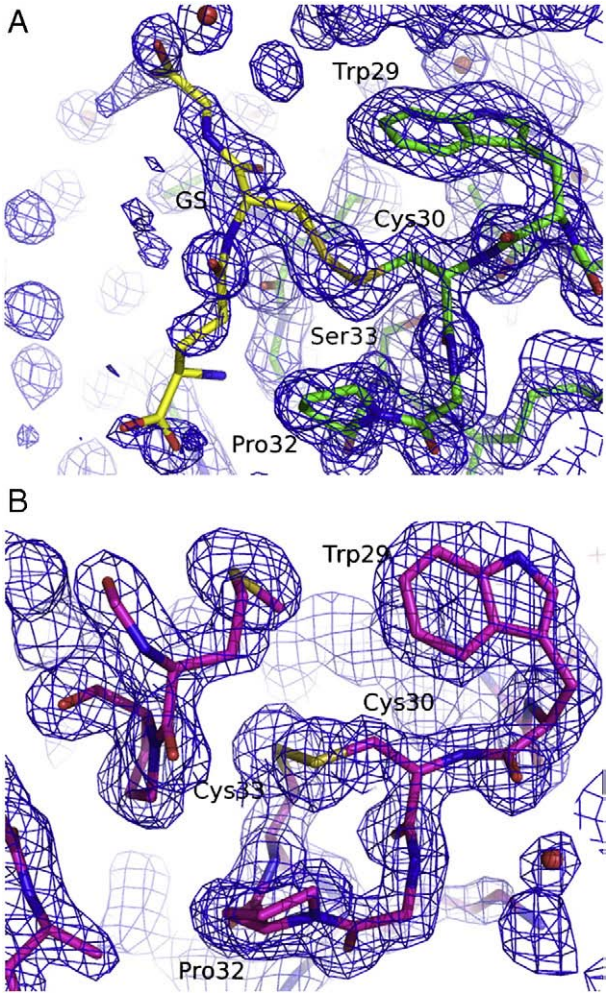

Fig. 1. The annealed omit electron density maps at 1.0 σ around the active sites of (A) gsTrx1C33S and (B) Trx1-ox. GSH is colored in yellow. The continuous electron density presents the disulfide bonds between Sγ atoms of Cys30 and the cysteinyl moiety of GSH in gsTrx1C33S, and Cys30–Cys33 in Trx1-ox. All structure figures are generated with PyMOL [36].

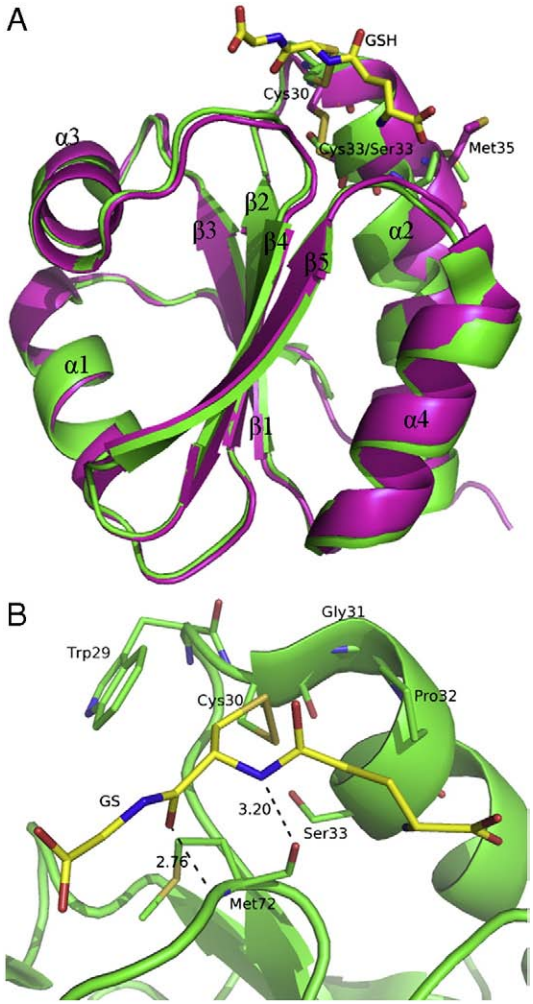

Fig. 2. Interactions and conformational changes upon GSH binding. (A) The overall structure superposition of Trx1-ox (in magenta) and gsTrx1C33S (in green). The active site cystein, Met35 and glutathionyl moiety are shown in stick style. (B) Interactions between Trx1C33S (in green) and GSH (yellow sticks). The active site WCGPS and Met72 are illustrated as sticks, and the two hydrogen bonds between the main chain of Met72 and cysteinyl moiety of GSH are indicated by black dashes with the distances in angstroms.

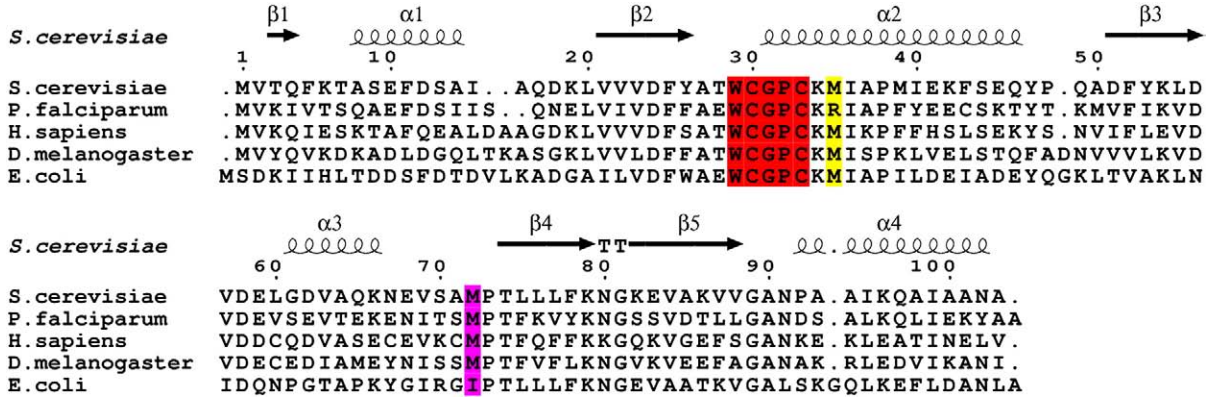

Fig. 3. Multialignment of thioredoxins from different species with Trx1's secondary structures indicated. The active site residues, the residue involved in GSH binding, and the distinguishing residue for various kinetic parameters are highlighted in red, magenta and yellow, respectively. The alignment was performed using CLUSTAL X [37] and the figure was prepared with ESPript [38].

indicating this region is critical to the reduction activity. The side chain conformational changes in the region of the redox active center due to different redox states or active site mutations have been observed in human hTrx1, yeast Trx3 and *D. melanogaster* DmTrx2 [31,32,35]. However, these changes are located at the region before the first active site cysteine, rather than the segment succeeding the second cysteine. Thus the conformational changes in our structures are mainly due to glutathionylation, rather than redox switch or active site mutations.

3.2. Comparison of Trx1 to thioredoxins from other species reveals a single residue substitution varying their reduction activities towards GSSG

As mentioned previously, the GSSG reduction efficiency of yeast Trx system is similar to that from *E. coli*, *D. melanogaster* and *H. sapiens*, but much lower than that of *P. falciparum* pTrx system. Superposition of Trx1-ox against the structure of oxidized *P. falciparum* pTrx (PDB code: 1SYR), *E. coli* TrxA (PDB code: 2TRX), *D. melanogaster* DmTrx2 (PDB code: 1XWA) and human hTrx1 (PDB code: 1ERU) gives an overall Cα RMSD of 1.03 Å, 1.36 Å, 1.49 Å and 0.94 Å, respectively. Given such a similar overall structure shared by these Trxs, the local structural or sequence discrepancies might be responsible for their different k_2 values. Multialignment of these Trxs reveals a distinct residue Arg43 that differs *P. falciparum* pTrx from its homologs (Fig. 3). Remarkably, the corresponding residue of the highly conserved Met35 in Trx1 undergoes a significant conformational change upon GSH binding (Fig. 2B). The substitution of Met with a positively charged residue Arg could enforce the electrostatic interactions to the carboxyl group of GSSG glycinyl moiety. We hypothesized that the Met to Arg substitution will facilitate substrate binding at the expense of lower product release rate.

3.3. Mutation of Met35 to Arg35 affects the enzyme activity

To verify this hypothesis, the Trx1M35R mutant was constructed and purified. The DTNB reduction method was employed to determine the respective K_m and V_{max} values of the wild-type and M35R mutant as the substrate of Trr1 (see Materials and methods). The apparent K_m and k_{cat} values were determined by non-linear regression of Michaelis–Menten plots (OriginPro 7.5). The rate constant k_2 of the Trx1M35R mutant towards GSSG is about 2.5-fold to that of the wild-type. This value was further validated by varying the final concentration of Trx1/Trx1M35R from 5 to 20 μM.

By applying various concentrations of the substrate GSSG, we obtained the kinetic parameters for Trx1–GSSG reaction, which are in agreement with our hypothesis (Fig. 4A). Excess Trr1 was added to ensure that all oxidized Trx1 would be instantaneously converted to its reduced form, excluding this reaction being a rate-limiting step. The derived k_{cat}'/K_m' (which approximately equals the rate constant k_2 of Reaction 2) values fits well with those k_2 values

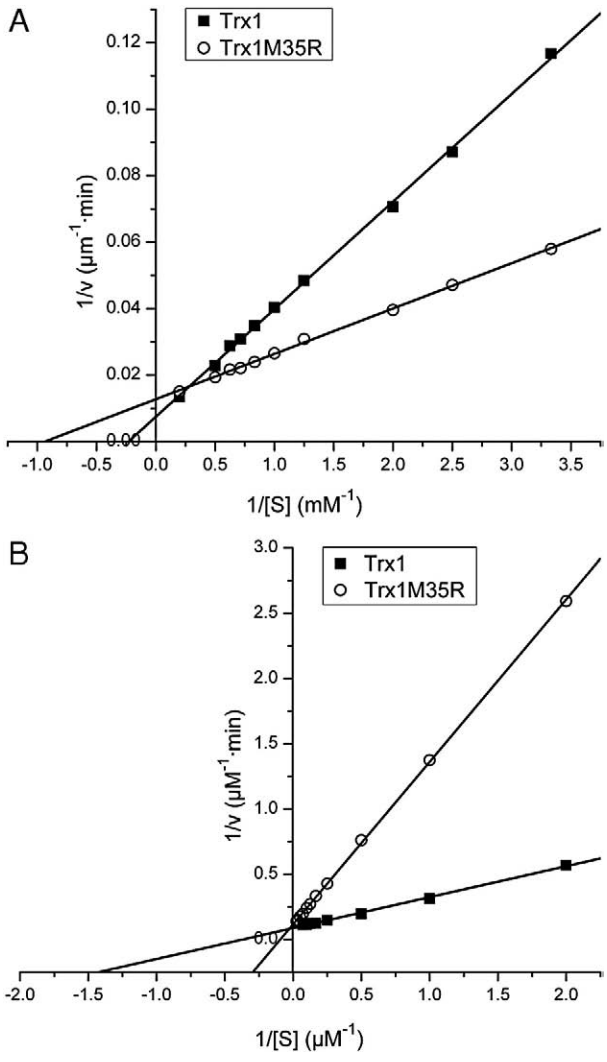

Fig. 4. Lineweaver–Burk double reciprocal plots of (A) Trx1 or Trx1M35R towards GSSG and (B) Trr1 towards Trx1 or Trx1M35R. The kinetic parameters are listed in Table 2.

Table 2
Kinetic constants for Trx1 and Trx1M35R in different reactions.

Protein	Trr1 (Reaction 1)			GSSG (Reaction 2)		
	K_m (μM)	k_{cat} (s^{-1})	k_{cat}/K_m ($\mu M^{-1}\ s^{-1}$)	K_m' (mM)	k_{cat}' (min^{-1})	k_{cat}'/K_m' ($mM^{-1}\ min^{-1}$)
Trx1	2.25 ± 0.16	17.79 ± 0.37	7.9	4.91 ± 0.23	29.44 ± 0.91	6
Trx1M35R	12.33 ± 0.63	15.63 ± 0.40	1.27	1.15 ± 0.04	16.24 ± 0.23	14

obtained by the above method (Table 2). Compared to the wild-type, Trx1M35R has a lower K_m' towards GSSG (about 1/5) and a lower turnover number k_{cat}' (about 1/2), resulting in an increased catalytic efficiency k_{cat}'/K_m' at a factor of 2.3 (Table 2). Taken together, the elevated reaction rate constant k_2 of the M35R mutant is contributed by the significant increase of its affinity to GSSG, despite that the k_{cat}' is decreased.

Notably, compared to the wild-type of Trx1, the K_m value of Trr1 towards Trx1M35R is increased to about 5–6 folds while k_{cat} is decreased marginally, leading to a decreased k_{cat}/K_m at a factor of 6–7 (Fig. 4B and Table 2). According to the Trr–Trx complex model proposed in our previous report [19], residue Met35 contributes to the hydrophobic interactions at the interface between Trr1 and Trx1. The M35R substitution will alter these interactions, resulting in a lower affinity of Trx1M35R to Trr1 and a higher K_m value.

3.4. Formation of the Trx-SG intermediate is the rate-limiting step during GSSG reduction

Early reports underestimated the *in vivo* significance of thioredoxin-based GSSG reduction based on it low reaction efficiency [14]. However, this reaction in the malaria parasite *P. falciparum* was revisited, despite being simplified as a chemical reaction characterized by the rate constant k_2 [9] (see Reaction 2). Based on the structural comparison in combination with kinetic analyses presented in this work, we suggest that Trx-SG formation is the rate-limiting step of the Trx system-driven GSSG reduction as shown in Reaction 3.

$$\mathrm{Trx} + \mathrm{GSSG} \overset{\mathrm{GSH}}{\uparrow} \rightarrow \mathrm{Trx-SG} \rightarrow \mathrm{Trx} + \mathrm{GSH} \qquad \text{(Reaction 3)}$$

First, GSSG oxidizes the reduced Trx1 into the Cys30-glutathionylated form accompanying with release of a reduced glutathione GSH. This step of GSSG binding to Trx1 is determinant to the K_m' value, which is in the rank of millimolar. The high value is probably due to the absence of sufficient interactions for GSSG binding. Nevertheless, the crystal structure of gsTrx1C33S reveals large conformational changes at helix α2 including Met35 upon glutathionylation, which mimics the first step of GSSG binding. A single mutation of Met35Arg will facilitate the binding of the negatively charged GSSG, resulting in a significant decrease of K_m' value towards GSSG.

Second, Cys33 attacks the mixed disulfide of Trx1Cys30-SG to release another reduced glutathione GSH at the cost of the oxidation of Trx1, which will be turned-over by Trr1. The second step could be characterized by the apparent turnover number k_{cat}', giving a k_{cat}'/K_m' value similar to the rate constant k_2 determined independently in this study. As indicated in the structures, the region around Met35 will shift to the opposite following glutathionylation of Cys30, leading to a weaker interaction with the glycinyl carboxyl group of GSH for the release of another reduced glutathione.

In conclusion, the reduction efficiency of Trx system-driven GSSG reduction is largely determined by the affinity of Trx towards GSSG, which is significantly influenced by the property of the residue corresponding to Met35 in Trx1. The present crystal structures and activity assays gave us more insights into the mechanism of Trx system-driven GSSG reduction.

Acknowledgments

This work was supported by the Ministry of Science and Technology of China (Projects 2006CB910202 and 2006CB806501), the National Natural Science Foundation of China (Programs 30670461 to YXC, 30870490 to CZZ), the Ministry of Education of China (Talents project of new century NCET-06-0374 and Program PRA B07-02 to YXC).

References

[1] T.C. Laurent, E.C. Moore, P. Reichard, Enzymatic synthesis of deoxyribonucleotides. IV. Isolation and characterization of thioredoxin, the hydrogen donor from *Escherichia coli* B, J. Biol. Chem. 239 (1964) 3436–3444.
[2] J. Chartron, C. Shiau, C.D. Stout, K.S. Carroll, 3′-Phosphoadenosine-5′-phosphosulfate reductase in complex with thioredoxin: a structural snapshot in the catalytic cycle, Biochemistry 46 (2007) 3942–3951.
[3] H.Y. Kim, J.R. Kim, Thioredoxin as a reducing agent for mammalian methionine sulfoxide reductases B lacking resolving cysteine, Biochem. Biophys. Res. Commun. 371 (2008) 490–494.
[4] M.I. Berggren, B. Husbeck, B. Samulitis, A.F. Baker, A. Gallegos, G. Powis, Thioredoxin peroxidase-1 (peroxiredoxin-1) is increased in thioredoxin-1 transfected cells and results in enhanced protection against apoptosis caused by hydrogen peroxide but not by other agents including dexamethasone, etoposide, and doxorubicin, Arch. Biochem. Biophys. 392 (2001) 103–109.
[5] A. Holmgren, Reduction of disulfides by thioredoxin. Exceptional reactivity of insulin and suggested functions of thioredoxin in mechanism of hormone action, J. Biol. Chem. 254 (1979) 9113–9119.
[6] A. Holmgren, Thioredoxin and glutaredoxin systems, J. Biol. Chem. 264 (1989) 13963–13966.
[7] A. Meister, M.E. Anderson, Glutathione, Annu. Rev. Biochem. 52 (1983) 711–760.
[8] I. Carlberg, B. Mannervik, Glutathione reductase, Methods Enzymol. 113 (1985) 484–490.
[9] S.M. Kanzok, A. Fechner, H. Bauer, J.K. Ulschmid, H.M. Muller, J. Botella-Munoz, S. Schneuwly, R. Schirmer, K. Becker, Substitution of the thioredoxin system for glutathione reductase in *Drosophila melanogaster*, Science 291 (2001) 643–646.
[10] S.M. Kanzok, R.H. Schirmer, I. Turbachova, R. Iozef, K. Becker, The thioredoxin system of the malaria parasite *Plasmodium falciparum*. Glutathione reduction revisited, J. Biol. Chem. 275 (2000) 40180–40186.
[11] Z.R. Gan, Yeast thioredoxin genes, J. Biol. Chem. 266 (1991) 1692–1696.
[12] H.Z. Chae, S.J. Chung, S.G. Rhee, Thioredoxin-dependent peroxide reductase from yeast, J. Biol. Chem. 269 (1994) 27670–27678.
[13] J.R. Pedrajas, E. Kosmidou, A. Miranda-Vizuete, J.A. Gustafsson, A.P. Wright, G. Spyrou, Identification and functional characterization of a novel mitochondrial thioredoxin system in *Saccharomyces cerevisiae*, J. Biol. Chem. 274 (1999) 6366–6373.
[14] E.G. Muller, A glutathione reductase mutant of yeast accumulates high levels of oxidized glutathione and requires thioredoxin for growth, Mol. Biol. Cell 7 (1996) 1805–1813.
[15] E.O. Garrido, C.M. Grant, Role of thioredoxins in the response of *Saccharomyces cerevisiae* to oxidative stress induced by hydroperoxides, Mol. Microbiol. 43 (2002) 993–1003.
[16] E.W. Trotter, C.M. Grant, Non-reciprocal regulation of the redox state of the glutathione–glutaredoxin and thioredoxin systems, EMBO Rep. 4 (2003) 184–188.
[17] D. Nikitovic, A. Holmgren, S-nitrosoglutathione is cleaved by the thioredoxin system with liberation of glutathione and redox regulating nitric oxide, J. Biol. Chem. 271 (1996) 19180–19185.
[18] Y. Zhang, R. Bao, C.Z. Zhou, Y. Chen, Expression, purification, crystallization and preliminary X-ray diffraction analysis of thioredoxin Trx1 from *Saccharomyces cerevisiae*, Acta Crystallogr., Sect F Struct. Biol. Cryst. Commun. 64 (2008) 323–325.
[19] Z. Zhang, R. Bao, Y. Zhang, J. Yu, C.Z. Zhou, Y. Chen, Crystal structure of *Saccharomyces cerevisiae* cytoplasmic thioredoxin reductase Trr1 reveals the structural basis for species-specific recognition of thioredoxin, Biochim. Biophys. Acta 1794 (2009) 124–128.
[20] X.C. Lou, Y.R. Zhang, R. Bao, C.Z. Zhou, Y. Chen, Purification, crystallization and preliminary X-ray diffraction analysis of *yeast* glutathionylated Trx1 C33S mutant, Acta Cryst. F 65 (2009) 39–41.
[21] A.G. Leslie, The integration of macromolecular diffraction data, Acta Crystallogr., D Biol. Crystallogr. 62 (2006) 48–57.
[22] K. Diederichs, P.A. Karplus, Improved R-factors for diffraction data analysis in macromolecular crystallography, Nat. Struct. Biol. 4 (1997) 269–275.

[23] E. Potterton, P. Briggs, M. Turkenburg, E. Dodson, A graphical user interface to the CCP4 program suite, Acta Crystallogr., D Biol. Crystallogr. 59 (2003) 1131–1137.
[24] R. Bao, Y. Chen, Y.J. Tang, J. Janin, C.Z. Zhou, Crystal structure of the yeast cytoplasmic thioredoxin Trx2, Proteins 66 (2007) 246–249.
[25] A.A. Vagin, M.N. Isupov, Spherically averaged phased translation function and its application to the search for molecules and fragments in electron-density maps, Acta Crystallogr., D Biol. Crystallogr. 57 (2001) 1451–1456.
[26] G.N. Murshudov, A.A. Vagin, E.J. Dodson, Refinement of macromolecular structures by the maximum-likelihood method, Acta Crystallogr., D Biol. Crystallogr. 53 (1997) 240–255.
[27] P. Emsley, K. Cowtan, Coot: model-building tools for molecular graphics, Acta Crystallogr., D Biol. Crystallogr. 60 (2004) 2126–2132.
[28] I.W. Davis, A. Leaver-Fay, V.B. Chen, J.N. Block, G.J. Kapral, X. Wang, L.W. Murray, W.B. Arendall 3rd, J. Snoeyink, J.S. Richardson, D.C. Richardson, MolProbity: all-atom contacts and structure validation for proteins and nucleic acids, Nucleic Acids Res. 35 (2007) W375–383.
[29] A. Holmgren, M. Bjornstedt, Thioredoxin and thioredoxin reductase, Methods Enzymol. 252 (1995) 199–208.
[30] A.S. Pinheiro, G.C. Amorim, L.E. Netto, F.C. Almeida, A.P. Valente, NMR solution structure of the reduced form of thioredoxin 1 from *Sacharomyces cerevisiae*, Proteins 70 (2008) 584–587.
[31] A. Weichsel, J.R. Gasdaska, G. Powis, W.R. Montfort, Crystal structures of reduced, oxidized, and mutated human thioredoxins: evidence for a regulatory homodimer, Structure 4 (1996) 735–751.
[32] M.C. Wahl, A. Irmler, B. Hecker, R.H. Schirmer, K. Becker, Comparative structural analysis of oxidized and reduced thioredoxin from *Drosophila melanogaster*, J. Mol. Biol. 345 (2005) 1119–1130.
[33] A. Holmgren, B.O. Soderberg, H. Eklund, C.I. Branden, Three-dimensional structure of *Escherichia coli* thioredoxin-S2 to 2.8 A resolution, Proc. Natl. Acad. Sci. U. S. A. 72 (1975) 2305–2309.
[34] J. Yu, N.N. Zhang, P.D. Yin, P.X. Cui, C.Z. Zhou, Glutathionylation-triggered conformational changes of glutaredoxin Grx1 from the yeast *Saccharomyces cerevisiae*, Proteins 72 (2008) 1077–1083.
[35] R. Bao, Y. Zhang, C.Z. Zhou, Y. Chen, Structural and mechanistic analyses of yeast mitochondrial thioredoxin Trx3 reveal putative function of its additional cysteine residues, Biochim. Biophys. Acta 1794 (4) (2009) 716–721.
[36] W.L. DeLano, The PyMOL User's Manual, Palo Alto, CA, USA, 2002.
[37] J.D. Thompson, D.G. Higgins, T.J. Gibson, CLUSTAL W: improving the sensitivity of progressive multiple sequence alignment through sequence weighting, position-specific gap penalties and weight matrix choice, Nucleic Acids Res. 22 (1994) 4673–4680.
[38] P. Gouet, E. Courcelle, D.I. Stuart, F. Metoz, ESPript: analysis of multiple sequence alignments in PostScript, Bioinformatics 15 (1999) 305–308.